14

BNWL-1845-38
UC-23

Quarterly Report on the Strontium Heat Source Development Program, Advanced Systems and Materials Production Division for January - March 1978

by
H. T. Fullam

April 1978

Pacific Northwest Laboratory
Richland, Washington 99352
Operated for the
U.S. Department of Energy
by

Battelle
Memorial Institute

BNWL-1845-38

NOTICE

This report was prepared as an account of work sponsored by the United States Government. Neither the United States nor the Department of Energy, nor any of their employees, nor any of their contractors, subcontractors, or their employees, makes any warranty, express or implied, or assumes any legal liability or responsibility for the accuracy, completeness or usefulness of any information, apparatus, product or process disclosed, or represents that its use would not infringe privately owned rights.

The views, opinions and conclusions contained in this report are those of the contractor and do not necessarily represent those of the United States Government or the United States Department of Energy.

PACIFIC NORTHWEST LABORATORY
operated by
BATTELLE
for the
UNITED STATES DEPARTMENT OF ENERGY
Under Contract EY-76-C-06-1830

Printed in the United States of America
Available from
National Technical Information Service
United States Department of Commerce
5285 Port Royal Road
Springfield, Virginia 22151

Price: Printed Copy $____*; Microfiche $3.00

*Pages	NTIS Selling Price
001-025	$4.50
026-050	$5.00
051-075	$5.50
076-100	$6.00
101-125	$6.50
126-150	$7.00
151-175	$7.75
176-200	$8.50
201-225	$8.75
226-250	$9.00
251-275	$10.00
276-300	$10.25

BNWL-1845-38
UC-23

3 3679 00062 2144

QUARTERLY REPORT ON THE STRONTIUM HEAT SOURCE DEVELOPMENT PROGRAM, ADVANCED SYSTEMS AND MATERIALS PRODUCTION DIVISION FOR JANUARY-MARCH 1978

by
H.T. Fullam

April 1978

PACIFIC NORTHWEST LABORATORY
OPERATED BY
BATTELLE MEMORIAL INSTITUTE
FOR THE
U.S. DEPARTMENT OF ENERGY

SUMMARY

STRONTIUM HEAT SOURCE DEVELOPMENT PROGRAM

Work has started on a theoretical analysis of the possible consequences of a WESF $^{90}SrF_2$ capsule rupture in an ocean environment.

ORNL has begun work on sectioning the capsules from the 12,000 hr compatibility tests with WESF $^{90}SrF_2$. Examination of the Haynes Alloy 25 specimens which were exposed to WESF $^{90}SrF_2$ for 6000 hr has been completed. The 6000-hr specimens suffered much greater attack than the equivalent 1000-hr specimens. The chemical attack mechanisms appeared to vary depending on the exposure temperature, while the addition of Zr + ZrF_4 to the $^{90}SrF_2$ to simulate decay product buildup, produced a marked decrease in metal attack.

The preliminary design of the outer capsule for the $^{90}SrF_2$ heat source has been completed. Fabrication of prototype test capsules from AISI 1018 low carbon steel, as a stand-in for thermally aged Hastelloy S, is now underway. The prototype capsules will be subjected to the major $^{90}SrF_2$ heat source qualification test requirements (1000-bar hydrostatic pressure test, impact test, and puncture test) to determine the adequacy of the outer capsule design.

CONTENTS

LIST OF FIGURES

LIST OF TABLES

STRONTIUM HEAT SOURCE DEVELOPMENT PROGRAM

H. H. Van Tuyl, Program Manager
H. T. Fullam, Principal Investigator
D. G. Atteridge
F. A. Simonen

At Hanford, strontium is separated from the high-level waste, converted to the fluoride, and doubly encapsulated in small, high-integrity containers for subsequent long-term storage. The fluoride conversion, encapsulation and storage take place in the Waste Encapsulation and Storage Facilities (WESF). The encapsulated strontium fluoride represents an economical source of ^{90}Sr if the WESF capsule can be licensed for heat source applications under anticipated use conditions. The objectives of this program are to obtain the data needed to license $^{90}SrF_2$ heat sources and specifically the WESF $^{90}SrF_2$ capsules. The information needed for licensing can be divided into three general task areas:

Task 1 - Chemical and Physical Properties of $^{90}SrF_2$
Task 2 - $^{90}SrF_2$ Compatibility Studies
Task 3 - Capsule Qualification and Licensing

Efforts are proceeding concurrently on all three tasks to obtain the required information.

TASK 1 - CHEMICAL AND PHYSICAL PROPERTIES OF $^{90}SrF_2$ (H. T. Fullam)

Work has started on a theoretical analysis of the possible consequences of a $^{90}SrF_2$ capsule rupture in an ocean environment. Two possible accident situations are being considered: capsule rupture in the deep ocean, and capsule rupture in the surface layer. In each case the accident is assumed to involve the rupture of a single WESF $^{90}SrF_2$ inner capsule containing 150,000 Ci of ^{90}Sr. The dissolution rate of the $^{90}SrF_2$ is assumed to be 300 µg Sr/hr-g Sr present, which is the highest dissolution rate observed with WESF-produced $^{90}SrF_2$ in seawater in dissolution rate tests carried out at PNL. The various models which have been proposed to describe point source dispersion in an ocean environment are being evaluated and the most appropriate model will be selected for evaluating the dispersion of $^{90}SrF_2$ in each accident situation. Current indications are that the three dimensional model

proposed by Okubo and Pritchard* is the most likely choice. PNL has used a modified version of the Okubo and Pritchard model to evaluate seabed disposal of high-level radioactive waste.

TASK 2 - $^{90}SrF_2$ COMPATIBILITY STUDIES

Long-Term Tests

All of the remaining compatibility tests are proceeding on schedule. No additional operating problems were encountered during the report period.

The capsules from the 12,000-hr tests with WESF $^{90}SrF_2$ were shipped to ORNL for sectioning and evaluation. The capsules have been removed from their Inconel-600 protective jackets, and sectionings of the capsules will begin in April.

ORNL has completed the metallography on the Haynes Alloy 25 specimens that were exposed to WESF $^{90}SrF_2$ for 6000 hr. Estimates of metal attack based on the photomicrographs obtained are presented in Table 1. The results obtained in the 1000-hr tests are also given in Table 1 for comparison purposes. Photomicrographs of selected specimens are shown in Figures 1-2. Metal attack was much greater in the 6000-hr specimens than in the corresponding 1000-hr specimens. Both the chemical attack and microstructural changes were much greater in the specimens exposed to $^{90}SrF_2$ at 1000°C than in the 600°C specimens. The attack mechanisms also appeared to vary with temperature (see Figure 1). Decreasing the S/V of the test couple resulted in greatly increased chemical attack at each temperature.

At 600°C, the test specimens suffered significant chemical attack which consisted primarily of general surface dissolution with formation of an adherent reaction layer. There was only slight indication of grain boundary attack. The reaction layer was leached away when the specimens were etched. The specimens tested at 600°C showed little indication of microstructural changes due to fluoride attack.

---

* A. Okubo and D. W. Pritchard, NYO-3109-40, September 1969.

TABLE 1. Estimated Attack of Haynes Alloy 25 Specimens Exposed to WESF $^{90}SrF_2$

Temp. °C	S/V[b] cm-1	Depth of Metal Affected,[a] mils: Chemical Attack 1000 Hr	Chemical Attack 6000 Hr	Change in Microstructure 1000 Hr	Change in Microstructure 6000 Hr
600	4.5	1	3	0	0
600	4.5	2	5	0	0
600	2.5	2	8	0	0
600[c]	4.5	<<1	1	0	0
800	4.5	5	10	10	16
800	4.5	4	11	6	18
800	2.5	18	30	10	34
800[c]	4.5	2	5	5	8
1000	4.5	6	12	8	18
1000	4.5	7	10	9	10
1000	2.5	10	20	12	25
1000[c]	4.5	5	4	3	8

[a] Estimated from photomicrographs
[b] S/V - the exposed metal surface-to-$^{90}SrF_2$ volume ratio of the test couple
[c] Zr + ZrF_4 added to the WESF $^{90}SrF_2$ to simulate 10 yr decay of the ^{90}Sr

At 800°C the test specimens suffered substantially greater attack than the 600°C specimens (see Figure 1). Chemical attack consisted primarily of selected leaching of alloy components with some grain boundary attack. The reaction zone contained free grains of unreacted metal. Microstructural changes consisted of a broad surface zone in which the normal grain boundary precipitates were partially depleted.

At 1000°C the chemical attack of the Haynes Alloy 25 specimens consisted primarily of extensive subsurface void formation and grain boundary attack (see Figure 1). Microstructural changes consisted of a broad surface zone in which the normal alloy precipitates were almost completely depleted.

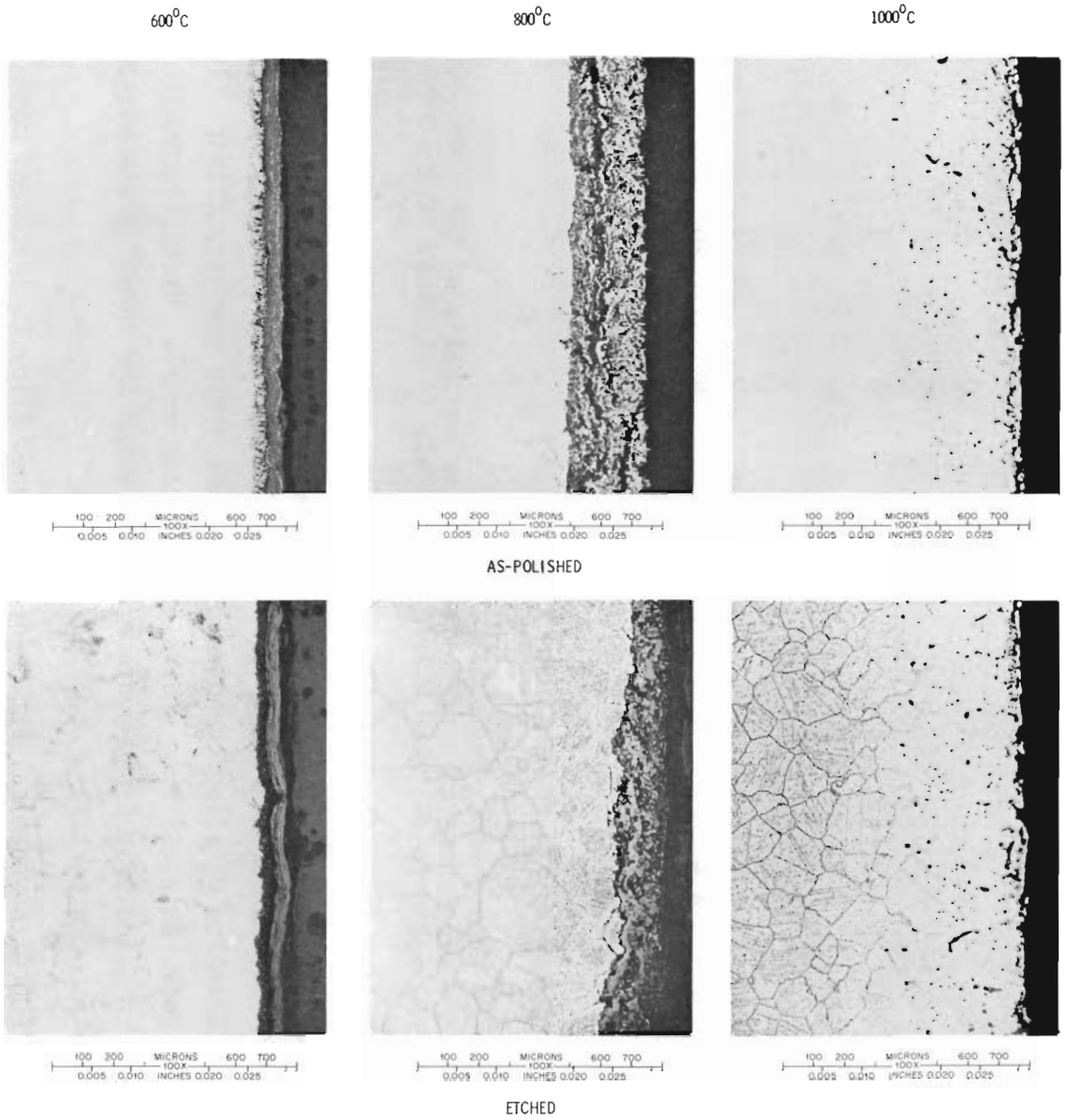

FIGURE 1: Haynes Alloy 25 Specimens Exposed to $^{90}SrF_2$ for 6000 Hr-S/V = 4.5 Cm^{-1}

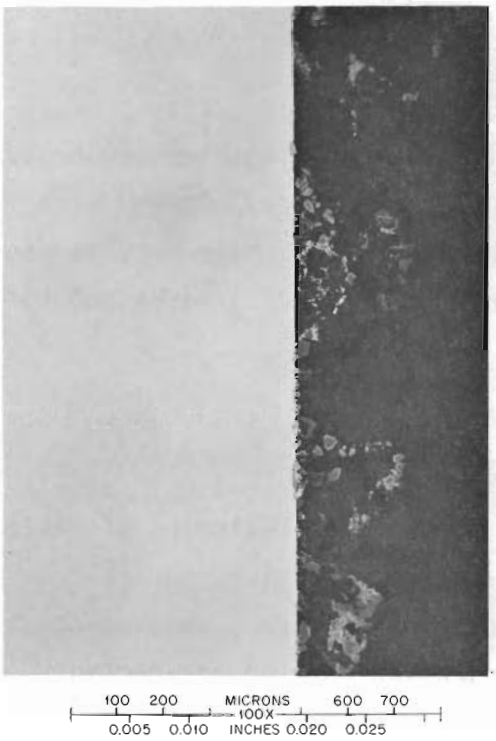

$600^{0}C$ - S/V = 4.5 cm^{-1}

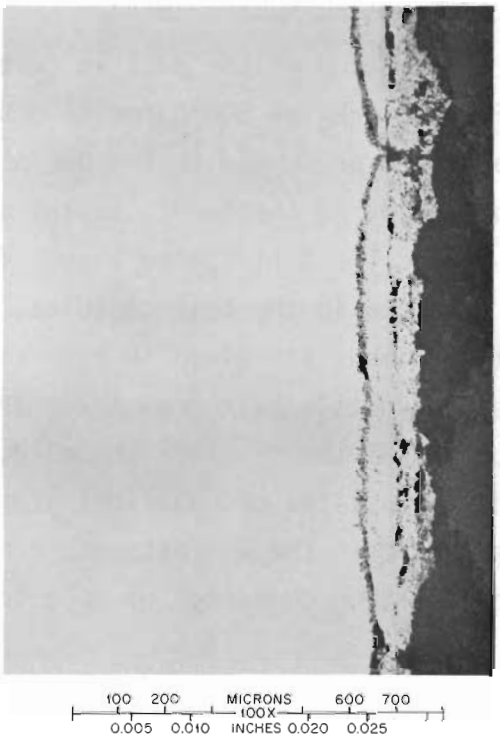

$800^{0}C$ - S/V = 4.5 cm^{-1}

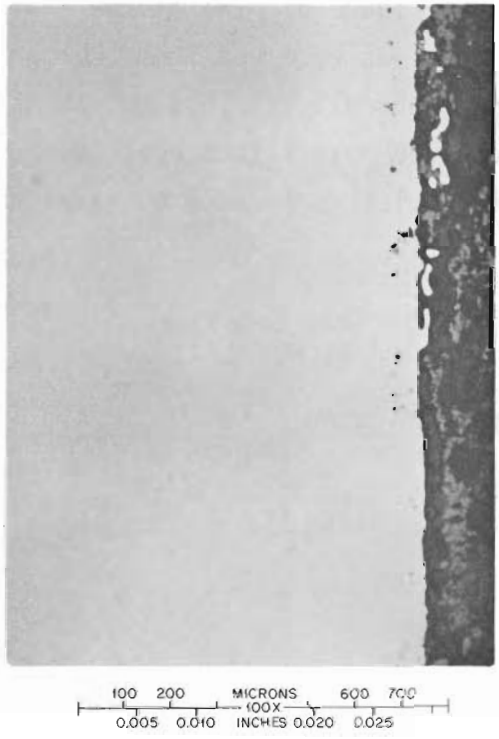

$1000^{0}C$ - S/V = 4.5 cm^{-1}

FIGURE 2: Haynes Alloy 25 Specimens Exposed for 6000 Hr to $^{90}SrF_2$ Containing $Zr+ZrF_4$

The addition of Zr + ZrF_4 to the WESF $^{90}SrF_2$ to simulate decay product buildup resulted in a marked decrease in metal attack at all three temperatures (see Figure 2). Both the chemical attack and microstructural changes were decreased by the addition of Zr and ZrF_4 to the fluoride. These results confirm those obtained with other test couples in which Zr + ZrF_4 was added to the fluoride.

Supplemental Screening Tests

Evaluation of the ductile cast iron specimens exposed to nonradioactive WESF-grade SrF_2 at 800°C for 4400 hr has been completed. Estimates of metal attack were presented in the December report and are also given in Table 2. Haynes Alloy 25 specimens, tested as reference samples, were also examined and showed the anticipated level of attack, indicating nothing unexpected had occurred in the test capsules. Micrographs of the ductile cast iron test specimens are given in Figures 3-5. The microstructures of the as-received ductile cast iron specimens are shown in Figure 3. The microstructure of the ferritic anneal ductile cast iron, as received from the vendor, consisted of spherical graphite nodules (spherulites) in a matrix of free ferrite. The microstructure of the as-received pearlitic anneal ductile cast iron consisted of spherical graphite nodules surrounded by envelopes

TABLE 2. Estimated Attack of Ductile Cast Iron Specimens Exposed to Nonradioactive SrF_2[a] at 800°C

Material	Depth of Metal Affected,[b] mils			
	Chemical Attack		Change in Microstructure	
	1500 hr	4400 hr	1500 hr	4400 hr
Pearlitic anneal ductile cast iron	3	4	2	5
Ferritic anneal ductile cast iron	3	4	2	7
Haynes alloy 25[c]	2	2	3	2

(a) The SrF_2 contained impurities similar to those found in WESF $^{90}SrF_2$.
(b) Estimated from photomicrographs.
(c) Tested as reference specimen.

"AS-RECEIVED"

AGED 4400 hr.

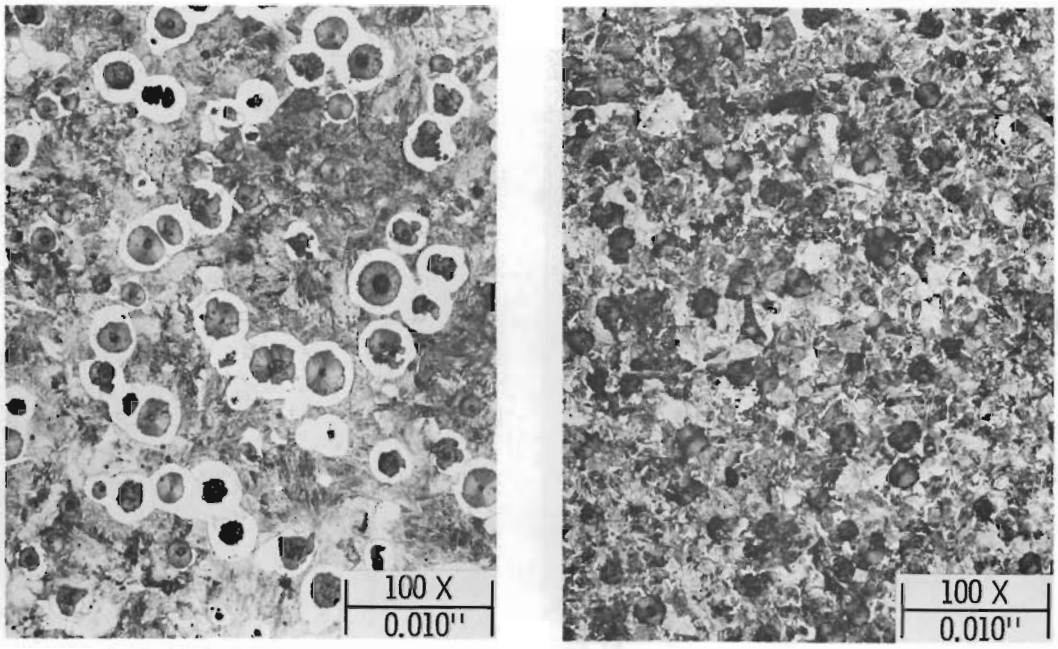

PEARLITIC ANNEAL DUCTILE CAST IRON

"AS-RECEIVED"

AGED 4400 hr.

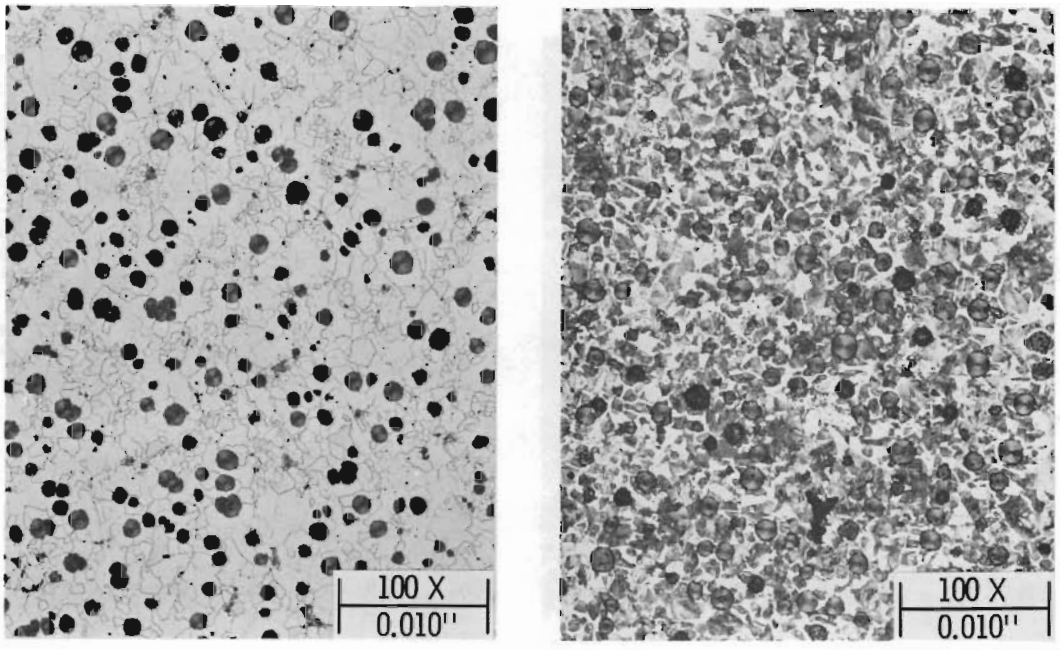

FERRITIC ANNEAL DUCTILE CAST IRON

FIGURE 3: The Microstructure of "As Received" and Thermally Aged (800°C) Specimens of Ductile Cast Iron

AS POLISHED

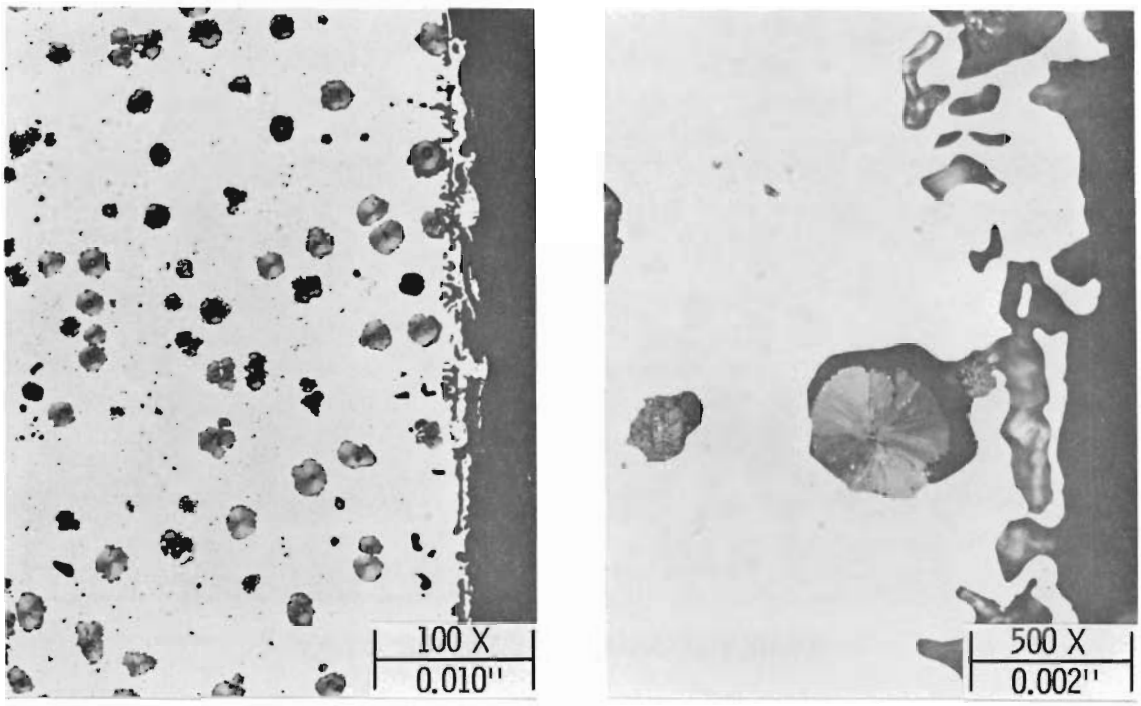

ETCHED

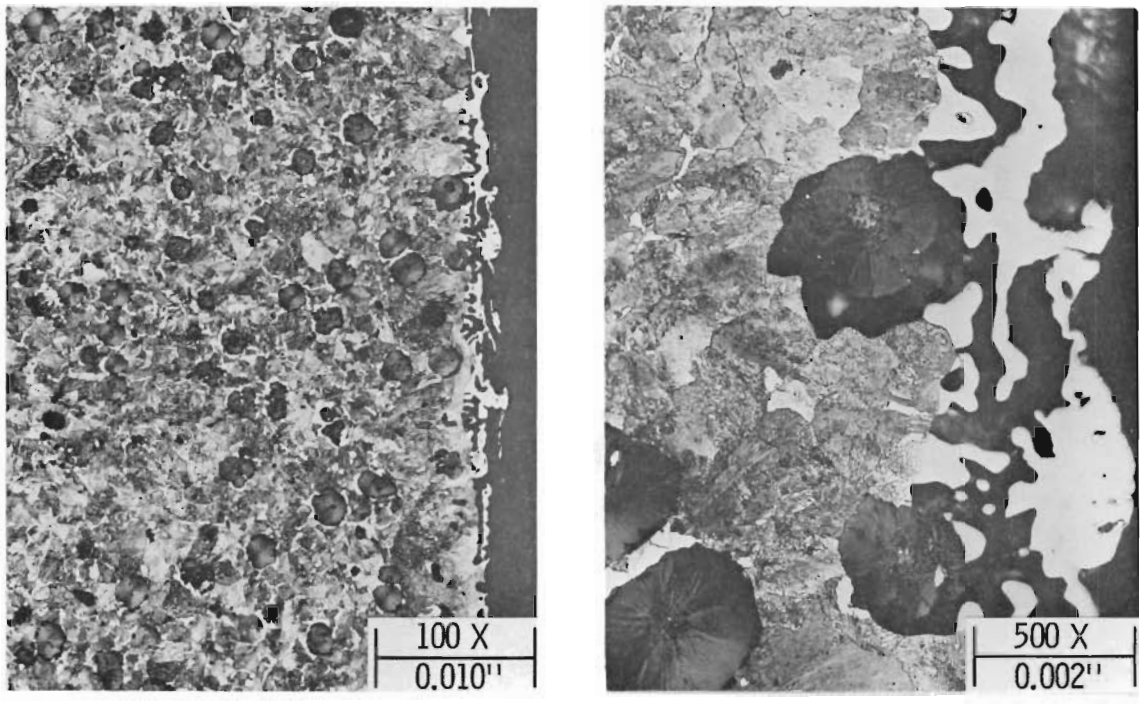

FIGURE 4: Pearlitic Anneal Ductile Cast Iron Specimen Exposed to WESF-grade Nonradioactive SrF_2 for 4400 Hr at 800°C

AS POLISHED

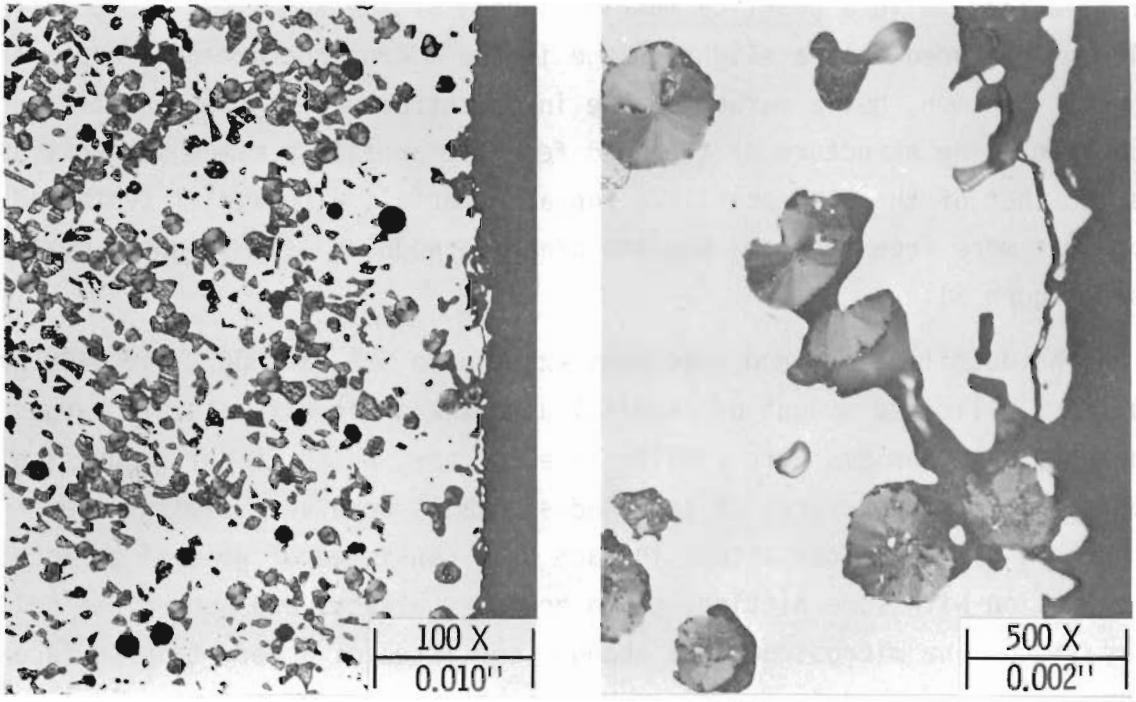

ETCHED

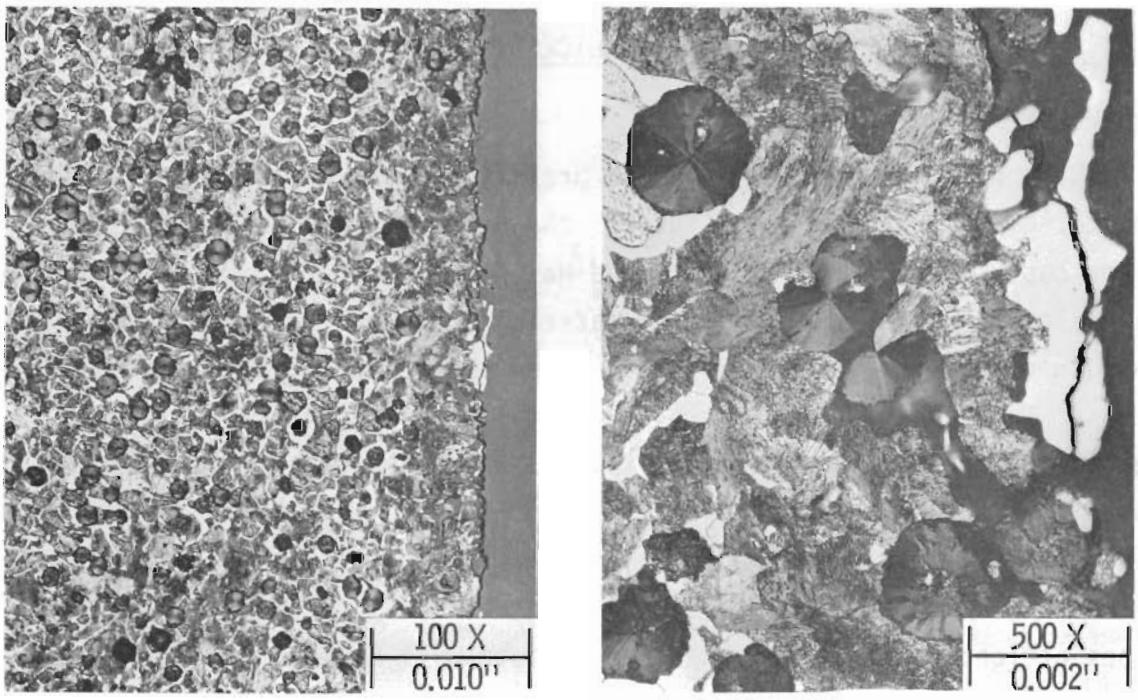

FIGURE 5: Ferritic Anneal Ductile Cast Iron Specimen Exposed to WESF-Grade Nonradioactive SrF_2 for 4400 Hr at 800°C

of free ferrite in a pearlite matrix. Aging of the specimens at 800°C for 4400 hr produced only a slight change in the microstructure of the pearlitic anneal specimen, but a marked change in the structure of the ferritic anneal specimen. The structure of the aged ferritic anneal specimen was very similar to that of the aged pearlitic anneal material, although it contained somewhat more free ferrite, and the graphite nodules were slightly smaller (see Figure 3).

The ductile cast iron specimens exposed to SrF_2 at 800°C for 4400 hr suffered a limited amount of chemical attack and microstructural changes. The attack mechanisms were similar in each case, which is not surprising since the microstructures of the aged specimens were very similar (see Figures 4-5). Chemical attack in each case consisted of general surface dissolution with some pitting, grain boundary attack, and subsurface void formation. The microstructural changes consisted of a very thin surface layer which appeared to contain a high concentration of free ferrite and a narrow inner zone which was depleted of free ferrite.

TASK 3 - CAPSULE QUALIFICATION AND LICENSING (D. G. Atteridge)

Capsule Design

Work has been completed on the preliminary design of the $^{90}SrF_2$ heat source. The heat source consists of the existing WESF Hastelloy C-276 inner capsule and a new PNL designed Hastelloy S outer capsule. Hastelloy S was selected as the outer capsule material from the four candidate materials because of its preferred properties after thermal aging at elevated temperatures. The new outer capsule has been designed so that it is capable of meeting the heat source qualification test requirements in both the as-fabricated and thermally aged conditions. The capsule was designed using a combination of a literature search for information on past heat source capsule design and computer simulation techniques to study the effects of the various types of loading sequences that the capsule will have to undergo.

F. A. Simonen has prepared a report for ASMP containing the major capsule design rationale and the results of the various computer simulation

programs used to evaluate the current design. The report is currently undergoing internal PNL review prior to being sent to ASMP. It is assumed that this report will be presented in a future quarterly report as soon as ASMP review is complete. A summary of its contents is given below.

The work on the capsule design determination is broken down into two sections. The first of these sections contains the results for the simulation of the hydrostatic pressure test requirement of 1000 bars which essentially determined the wall thickness of the heat source outer capsule. The second section contains the results of the 30 foot drop-impact simulations which essentially determined the end closure configuration.

Pressure Test Simulation Results

The 14,500 psi external pressure requirement dictated a relatively thick-wall capsule. It was, therefore, essential to estimate failure pressures with some precision so that an unnecessary penalty did not result in terms of capsule size and weight. Unfortunately, design equations for thick-walled tubing in the wall thickness and pressure range of interest are decidedly lacking, as are experimental results for external collapse pressures. Thus, detailed finite element analyses were performed to evaluate geometric and material variables. Both the case of thin-walled tubing collapsed by an elastic instability mode and the case of thick-walled tubing collapsed after a general wall yielding were investigated.

The finite element computer code ADINA was used to study external pressure induced collapse of the outer capsule. The program allowed effects of plastic deformation, strain hardening in the plastic range, and capsule out-of-roundness to be studied. It was determined that a capsule with a wall thickness sufficient to withstand an external pressure of 1000 bars would fail as a result of the complete yielding of the wall, as thick-walled tubing is known to do, and not catastrophically through the formation of an elastic instability, as thin-walled tubing is known to do. In addition, it was determined that the wall thicknesses of interest resulted in a capsule relatively insensitive to tube imperfections, such as ovality, for the tube diameter of interest for this application. Thus, a thick-walled perfectly symmetrical tube section was used in determining the required capsule wall thickness.

The wall thickness design started out with a given inside diameter. The diameter that the capsule was designed around was 2.325 in. This inside diameter results in the gap between the heat source outer capsule and the inner WESF capsule being about one-half the gap between the existing WESF inner and outer capsule. The gap reduction was based on discussions with Rockwell Hanford Operations WESF personnel who report no problems in the assembly of inner capsules into outer capsules. The proposed gap width will result in an estimated temperature drop of 30°C between the inner and outer heat source capsule, assuming helium in the gap.

Two sets of wall thicknesses were determined during the computer simulation investigations. One set corresponded to the wall thickness needed for complete protection from any plastic yielding of the capsule wall while the other set corresponded to the point at which the complete wall has reached the plastic yielding condition. This latter condition must be reached in thick-walled tubes before tube collapse. Both sets of results are given in Tables 3 and 4 for the four candidate capsule materials, along with their assumed room temperature yield strengths. It was decided that, as the capsule wall would have to be in the completely plastic condition prior to noticeable capsule collapse, the use of the wall thickness necessary for the first plastic yielding of the inner wall would be too conservative. Thus, it was decided to use the complete plastic failure criterion wall thickness values and to add a safety factor on top of that value. The minimum wall thickness for Hastelloy S by this design standard would be 0.407 in.; we have designed our capsule prototype using a wall thickness of 0.45 in.

TABLE 3. Required Capsule Dimensions to Avoid Local Plastic Deformation at Capsule Inside Diameter for External Pressure of 14,500 psi (ID = 2.325 in.)

Material	Yield Strength psi	Outside Diameter inch	Wall Thickness inch
Hastelloy S	42,000	4.179	0.927
Hastelloy C-4	48,700	3.644	0.665
Inconel 625	42,000	4.179	0.927
Inconel 617	43,000	4.074	0.875

TABLE 4. Required Capsule Dimensions to Avoid Fully Plastic Condition of Capsule Wall for External Pressure of 14,500 psi (ID = 2.325 inch)

Material	Yield Strength psi	Outside Diameter inch	Wall Thickness inch
Hastelloy S	42,000	3.139	0.407
Hastelloy C-4	48,700	3.012	0.343
Inconel 625	42,000	3.139	0.407
Inconel 617	43,000	3.117	0.396

Capsule End Impact Test Simulation Results

The simulation results for the 30-ft drop-impact test, along with predetermined maximum weld penetration requirements, were used to determine the capsule closure end cap design. The weldment criterion that was used in the design of the end capsule was that the weld penetration depth would be limited to 0.1 in. or less, which is essentially the depth of weld currently used on the existing WESF capsules. This penetration depth was used as it corresponds to the maximum penetration depth achievable for TIG welding without the use of filler metal. The use of filler metal in a remote control welding operation such as in a hot cell greatly complicates the welding procedure and the welding equipment requirements, and is therefore to be avoided if at all possible.

The decision to use a partial penetration weld for capsule closure, (a 0.1 in. weld used to weld a cap to a 0.45 in. capsule wall) brought up the problem of low impact resistance for any of the standard capsule closure designs investigated in our literature search. The experimental results on partial penetration closure welds for both flat cap and screw caps showed weld failures and/or gross plastic deformation of the weld during impact testing. Therefore it was decided to design a new mechanically stabilized capsule closure configuration that would allow a shallow weld penetration and still be resistant to deformation during impact. It was decided that a simple mechanical interlocking type of joint would sufficiently suppress local buckling deformation at the end of the capsule during impact. A schematic of this interlocking design is shown in Figure 6. The impact resistance of this

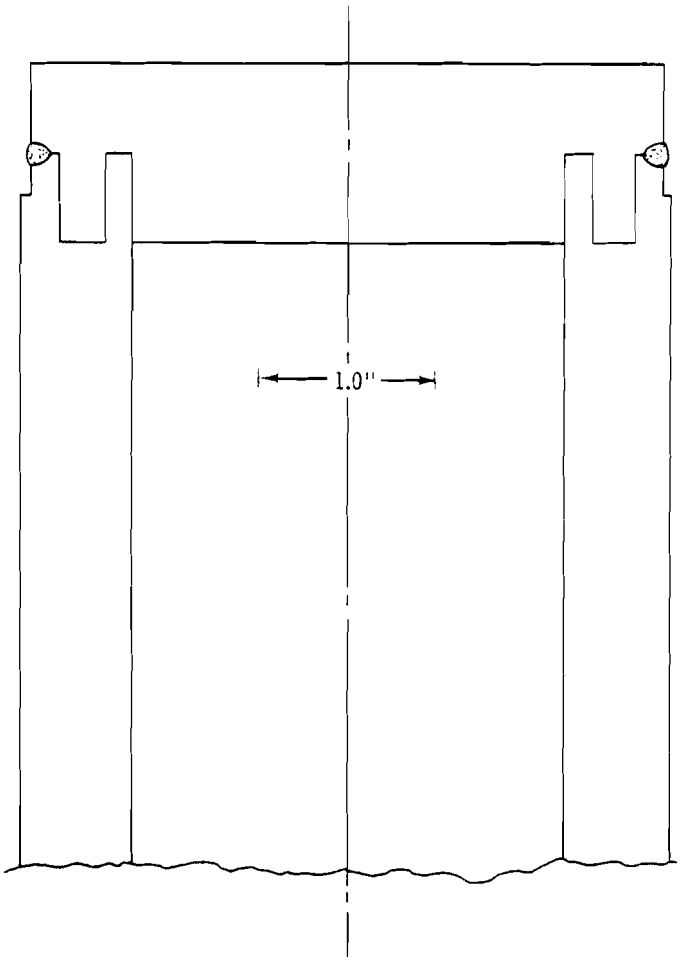

FIGURE 6. Schematic of Proposed Interlocking Outer Capsule Cap and Cap Weld

interlocking design, along with that of a standard design with the same weld penetration but without the interlocking feature, was determined through computer simulation techniques. The performance of these two end closure designs under impact conditions were evaluated using the finite element computer program HONDO.

The computer simulation results for a bottom impact situation for the non-interlocking end cap design are shown in Figure 7. It can be seen that considerable plastic deformation has taken place in both the capsule wall and the closure weld. In fact, it is estimated that the resultant plastic deformation predicted to be in the weld would be enough to cause fracture of the weldment and to possibly result in complete failure of the weld. The simulation results for the interlocking end cap are shown in Figure 8. It is obvious that very

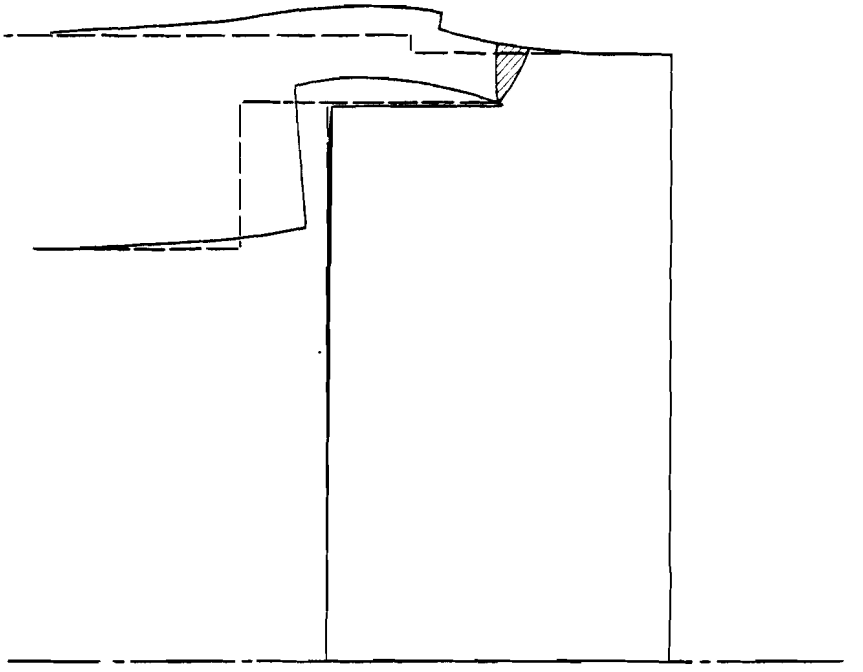

FIGURE 7. Predicted Deformation of Non-Interlocking End Cap for End Impact of 30-ft Drop

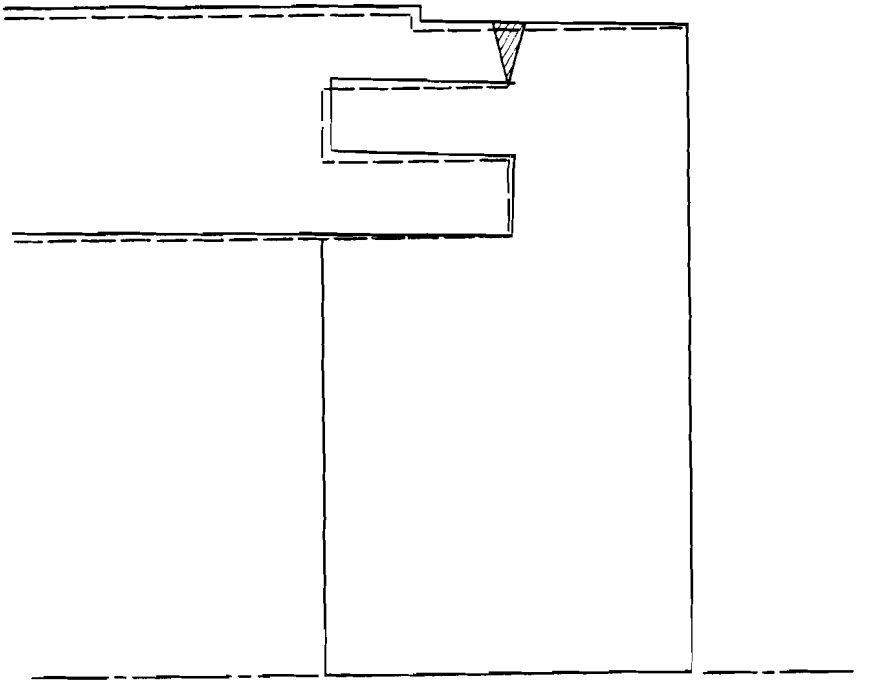

FIGURE 8. Predicted Deformation of Interlocking End Cap for End Impact of 30-ft Drop

little plastic deformation of the closure configuration has taken place. In fact the only noticeable effect was a slight rotation of the end cap mechanical strengthener, resulting in a slight rotation of the capsule wall. Essentially no plastic deformation of the closure weld took place.

A check of the interlocking end closure resistance to an external hydrostatic loading of 1000 bars using the computer program ADINA was also carried out. The results of the simulation indicated that stress at the closure weld location will not exceed 10,000 psi, which is well below the yield strength of the material. Thus, it is predicted that the heat source capsule will fail by wall buckling prior to any plastic deformation of the closure welds.

Prototype Heat Source Outer Capsule Design

The prototype capsule design essentially incorporated the 0.45 in. wall thickness determined for the Hastelloy S alloy by the hydrostatic test simulation and the interlocking end closure design determined to be resistant to impact loading. Figure 9 shows the fabrication drawings for the prototype capsule. The capsule essentially consists of a 20.7 in. long tube with an inside diameter of 2.325 in. and a wall thickness of 0.45 in. The end cap is essentially an 1.0 in. thick interlocking cap which will be TIG welded to the capsule body. No filler metal will be used in the welding operation. A comparison of the new heat source outer capsule dimensions with those of the current WESF capsule is given in Figure 10.

Capsule Design Test Program

PNL is planning to conduct a near-term impact and external pressure test program directed towards capsule design assurance. The objective of the program is to assure as much as possible that the chosen capsule design will meet all licensing test requirements after long-term elevated temperature aging of the prototype Hastelloy S capsules. It was decided that the program would use full size capsules fabricated out of a material that exhibits room temperature yield stress and impact energies near those expected to be found in the Hastelloy S after 10 years of service at 800°C. AISI 1018 low carbon steel was chosen for this application. It is expected to have a yield stress of between 40 and 50 ksi and an impact energy close to 30 ft-lb at room temperature. In

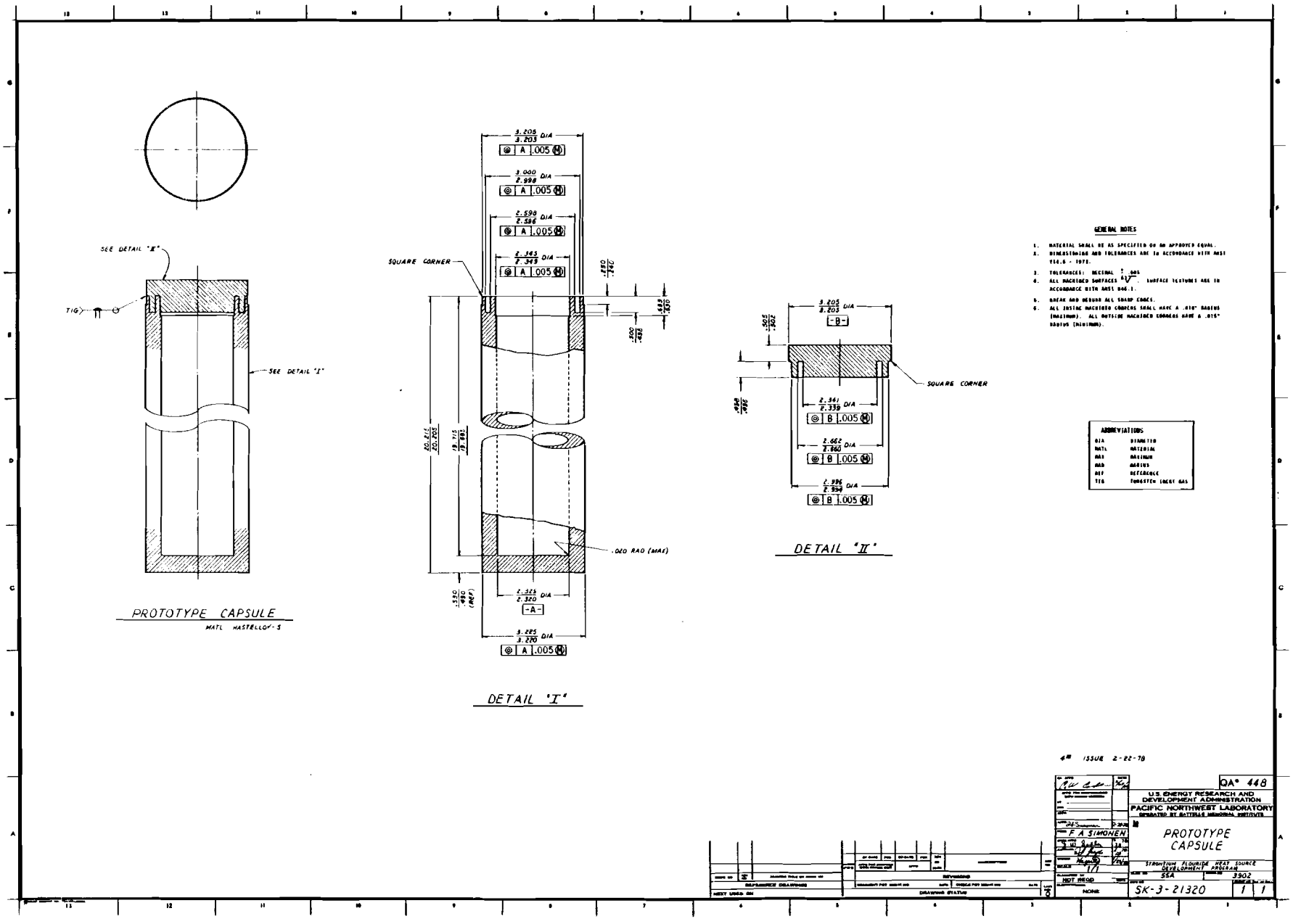

FIGURE 9. Prototype Pressure Test Capsule Having a 0.45 in. Wall

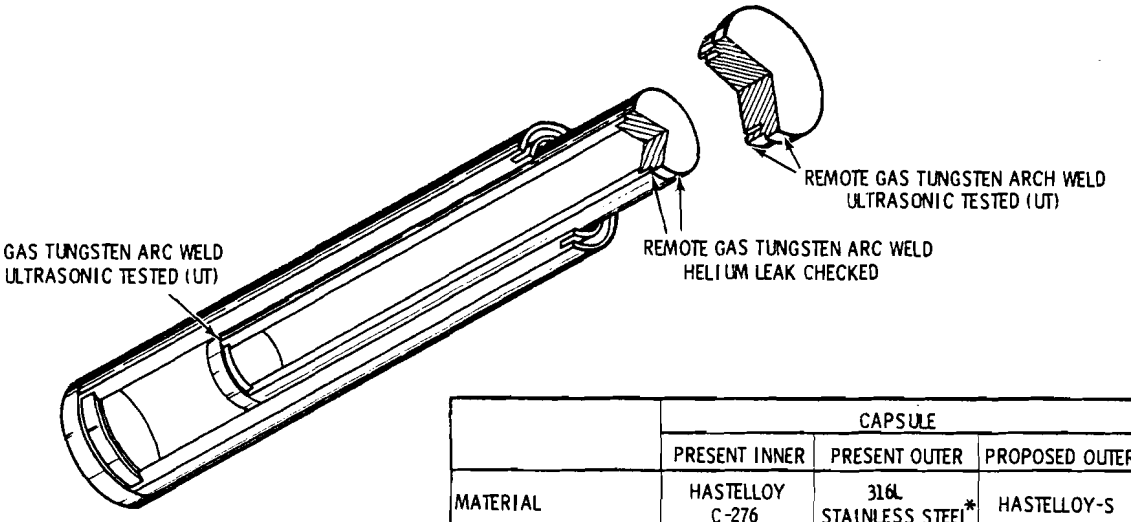

	CAPSULE		
	PRESENT INNER	PRESENT OUTER	PROPOSED OUTER
MATERIAL	HASTELLOY C-276	316L STAINLESS STEEL*	HASTELLOY-S
WALL THICKNESS, INCH	0.120	0.120	0.450
OUTSIDE DIAMETER, INCH	2.250	2.625	3.225
TOTAL LENGTH, INCH	19.500	20.100	20.720
TOTAL CAP THICKNESS, INCH	0.400	0.400	1.000

*SOME OF THE EARLY WESF $^{90}SrF_2$ CAPSULES USED HASTELLOY C-276 FOR THE OUTER CAPSULE

FIGURE 10. Proposed Outer Capsule for the $^{90}SrF_2$ Heat Source

addition it is available in heavy-walled tubing, and one can change its impact resistance over a considerable range by a change in temperature (see Figure 11).

It was decided that three different wall thickness capsules were needed in order to evaluate the capsule high pressure collapse prediction model. These included a wall thickness of 0.5 in. (close to the predicted capsule thickness) and one thicker and one thinner wall, 0.6 in. and 0.4 in., respectively. It is planned that these capsules will be tested in 1000 psi pressure steps from 10,000 psi to 20,000 psi, with a leak and dimensional check between each pressure step. These capsules will be used to check out the validity of the pressure collapse model. In addition, one 0.5 in. wall capsule will be tested at 1000 bars in order to allow an in-depth destructive as well as nondestructive analysis of a capsule tested at the required qualification test pressure. Several capsules with a wall thickness of 0.5 inch will also be used to

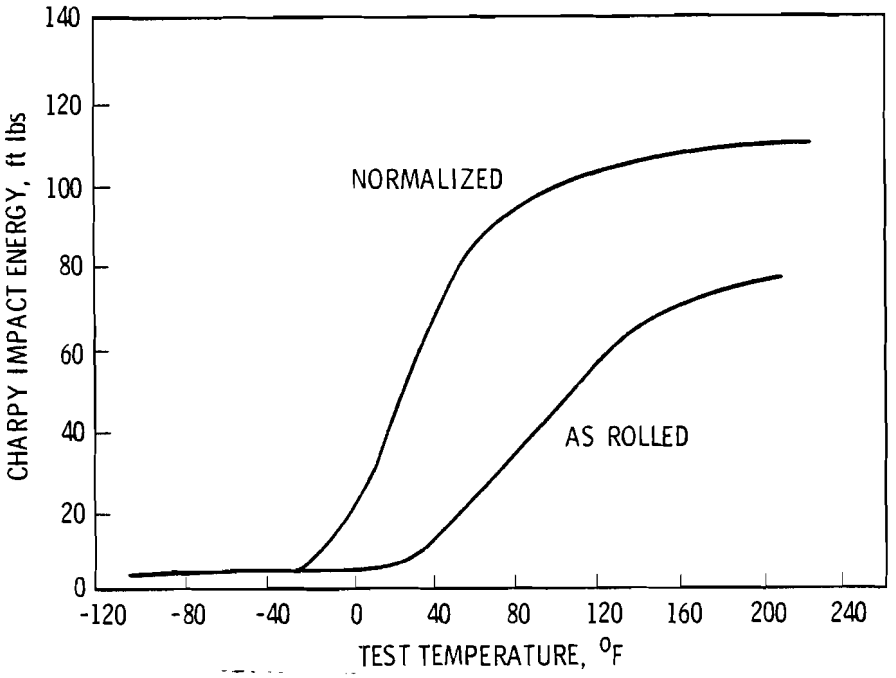

FIGURE 11. Charpy Impact Energy as a Function of Test Temperature for AISI 1018 Low Carbon Steel

determine the impact and puncture resistance of the capsule design. We are currently in the process of developing a test matrix that will allow evaluation of the impact resistance of the test capsule design as a function of material impact resistance and weld depth penetration.

The AISI 1018 low carbon steel capsules required for the test programs have been machined. In addition, several smaller specimens for weld parameter determination and mechanical property evaluation are currently being machined. As soon as the welding parameters are developed, the capsules will be welded and testing will begin.

Tensile Test Results for Hastelloy S and C-4 Alloys

The Stellite Division of Cabot Corporation supplied PNL with a series of failed tensile specimens from materials (Hastelloy S and Hastelloy C-4) that had been aged at various temperatures (800 to 1600°F) for various times (1,000 to 16,000 hr). The Stellite tensile specimens had gauge section diameters of 1/2 in. and were all tested at room temperature. PNL took the original failed tensile specimen halves and machined two sets of subsize tensile specimens

from them. The relationship between the original Stellite specimens and the subsequent PNL specimens is shown in Figure 12. PNL then tested these subsize tensile specimens at a variety of test conditions.

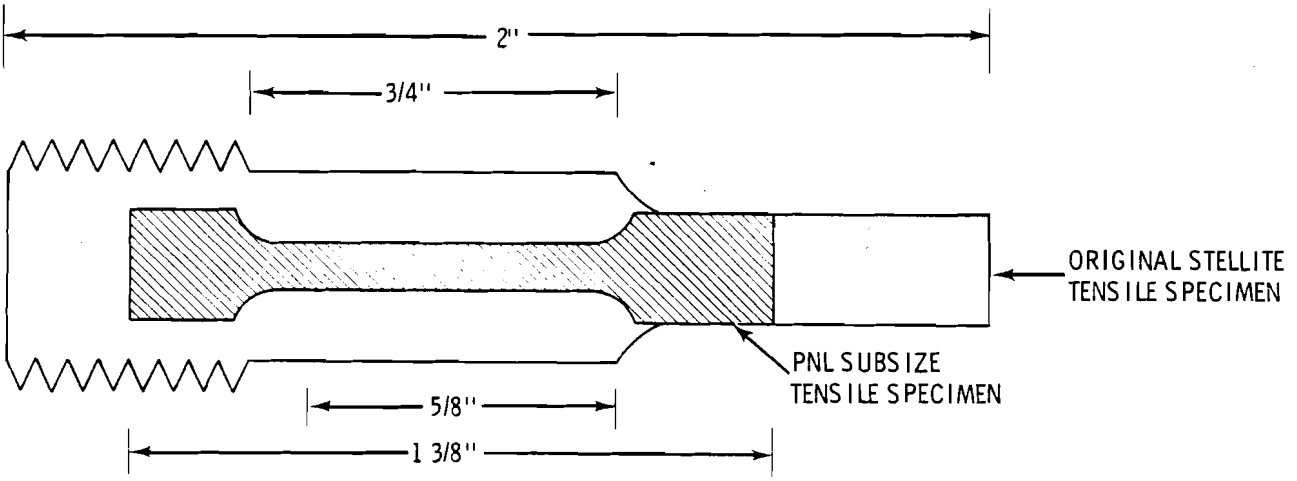

FIGURE 12. Schematic Showing the Relationship Between a Stellite Failed Tensile Specimen and the PNL Specimen Subsequently Machined from It

A complete set of specimens was tested at the test temperature to which it was exposed. The specimens in the remaining set were tested under three different conditions. One series was tested at 800°C to determine the effect of long-term intermediate temperature exposure prior to full activation of the heat source. Another series was tested at room temperature to assure that there were no gross differences between the resultant properties of the Stellite and PNL specimens. The rest of the specimens were tested at their original exposure temperature to assess the reliability of the evaluated temperature data generated in the testing of the first set of specimens.

Table 5 presents the results of the elevated temperature testing done at PNL on test specimens of Hastelloy C-4 and S material supplied by the Stellite Corporation. It can be seen that the elevated temperature data at and below 1200°F show good agreement between duplicate specimens while those tested at 1400 and 1600°F show considerable scatter for selected test conditions. The upper temperature test specimens exhibited very little, if any, work hardening

TABLE 5. Elevated Temperature Tensile Test Results for Hastelloy S and Hastelloy C-4

Exposure and Test Temperature	Exposure Hours	Stress, ksi		% Elongation		% Reduction of Area
		Yield	Ultimate	Uniform	Total	
			Hastelloy S			
800°F	1,000	44.3	110.9	48	54	64
	4,000	47.3	108.2	47	50	60.8
	8,000	49.0	111.6	48	52	58
	8,000	47.8	114.2	48	52	55
	16,000	52.7	114.3	46	50	57
1,000°F	1,000	65.5	128.4	37	39	45
	1,000	54.7	120.0	45	46	45
	4,000	88.3	144.8	31	35	52
	8,000	87.5	145.9	32	38	52
	16,000	57.8	98.5	42	49	42
	16,000	91.8	152.3	29	35	51
1,200°F	1,000	44.6	97.6	44	60	54
	1,000	44.1	99.5	42	59	53
	4,000	43.2	95.5	45	49	40
	8,000	45.2	96.0	40	38	41
	8,000	43.7	93.9	37	46	42
	16,000	44.3	95.1	35	42	43
1,400°F	1,000	40.0	66.1	16	51	55
	1,000	41.8	64.8	14	47	62
	4,000	40.3	67.7	17	50	57
	4,000	41.6	68.4	15	48	56
	8,000	41.0	71.9	16	52	57
	8,000	40.3	62.9	12	46	60
	16,000	42.8	75.3	17	48	53
	16,000	41.2	59.5	12	45	62
1,600°F	1,000	36.1	41.2	8	60	69
	1,000	32.2	34.0	3	63	89
	4,000	35.5	37.3	3	60	61
	4,000	31.9	32.4	3	61	86
	8,000	28.0	28.5	2	61	85
	8,000	37.5	38.6	3	66	85
	16,000	19.0	20.5	5	64	83
	16,000	34.3	35.1	3	59	87

TABLE 5 (cont'd)

Exposure and Test Temperature	Exposure Hours	Stress, ksi		% Elongation		% Reduction of Area
		Yield	Ultimate	Uniform	Total	
			Hastelloy C-4			
800°F	1,000	44.9	106.5	50	56	57
	4,000	45.4	110.2	52	56	57
	4,000	48.8	112.5	51	56	60
	8,000	45.2	112.3	53	57	60
	16,000	51.1	119.0	52	56	56
	16,000	48.9	115.1	49	54	60
1,000°F	1,000	89.3	153.9	32	37	43
	4,000	89.1	103.0	25	26	27
	8,000	98.8	114.4	12	13	15
	16,000	81.1	107.4	9.5	10	7
1,200°F	1,000	69.2	115.1	25	27	26
	4,000	55.2	104.1	27	29	27
	4,000	55.3	102.6	27	28	30
	8,000	65.3	117.4	23	24	26
	8,000	67.0	112.9	18	19	33
	16,000	72.2	119.4	17	18	19
1,400°F	1,000	44.8	67.7	13	59	55
	1,000	44.1	68.4	13	47	51
	4,000	43.3	75.3	19	50	51
	4,000	43.0	68.8	12	45	56
	8,000	44.1	79.6	18	45	46
	8,000	44.8	72.6	15	45	55
	16,000	44.5	73.9	14	46	52
	16,000	44.6	68.2	10	42	52
1,600°F	1,000	36.7	38.1	7	62	84
	1,000	36.1	38.6	4	59	88
	4,000	36.4	40.3	9	60	85
	4,000	38.3	40.5	3	82	86
	8,000	40.3	46.8	9	52	62
	8,000	58.9(1)	62.2	23	54	58
	16,000	38.7	45.4	9	51	74
	16,000	36.7	41.0	11	51	67

(1) Tested at a strain rate of 0.926 cm/min

capability with the result that their mechanical properties are more controlled by small changes in surface contour, grain structure, and other defects such as residual casting defects, than the lower temperature specimens. Thus, it is not too surprising that these small subsized specimens exhibited considerable data scatter in given instances. The overall data trends vary little from the elevated temperature test results presented previously in the July-September 1977 quarterly report.

The limited testing performed on specimens tested at 800°C after being subjected to the maximum embrittling lower temperature exposure conditions (see Table 6) indicates that they act almost as if they had never received the low temperature exposure after a short 1/2 hour soak prior to the 800°C testing. The data in Table 7 show that there is relatively good agreement between the room temperature data from the PNL specimens and the Stellite specimens.

TABLE 6. 800°C Tensile Test Results for Hastelloy S and Hastelloy C-4

Exposure Temperature	Exposure Hours	Stress, ksi		% Elongation		% Reduction of Area
		Yield	Ultimate	Uniform	Total	
			Hastelloy S			
800°F	1,000	38.9	56.9	9	59	85
	16,000	40.3	50.8	7	60	87
1,000°F	4,000	40.8	57.3	10	68	87
1,200°F	1600	40.5	57.5	9	59	78
			Hastelloy C-4			
800°F	1,000	40.7	53.0	10	52	70
1,000°F	16,000	41.0	55.2	8	35	41
1,200°F	16,000	45.7	57.2	7	32	41

TABLE 7. Room Temperature Tensile Test Results for Hastelloy S and Hastelloy C-4

Exposure Temperature	Exposure Hours	Specimen Size	Stress, ksi Yield	Stress, ksi Ultimate	% Elongation Uniform	% Elongation Total	% Reduction of Area
		Hastelloy S					
800°F	4,000	Standard[1]	55.5	129.9		60	66
	4,000	Subsize[1]	66.8	139.4	47	53	69
1,000°F	8,000	Standard	108.2	180.8		38	49
	8,000	Subsize	117.0	196.5	38	43	57
1,200°F	4,000	Standard	56.4	125.8		54	53
	4,000	Subsize	67.0	138.4	43	47	54
		Hastelloy C-4					
800°F	8,000	Standard	60.0[2]	128.8		59	63
	8,000	Subsize	78.4	145.9	47	54	69
1,000°F	1,000	Standard	113.7	191.9		42	51
	1,000	Subsize	115.7	203.3	37	43	52
	4,000	Standard	113.0	194.6		40	51
	4,000	Subsize	121.3	215.6	36	41	50
	8,000	Standard	116.1	197.0		35	47
	8,000	Subsize	120.7	208.9	37	39	46
1,200°F	1,000	Standard	82.9	156.1		45	47
	1,000	Subsize	88.2	167.8	41	44	46

[1] Standard 0.5 in. diameter specimens tested by the Stellite Division of the Cabot Corporation; subsize 0.11 in. diameter speciments tested by PNL.

[2] Tested at a strain rate of 0.926 cm/min.

Oxidation of Hastelloy S and Hastelloy C-4

Long-term tests to measure the oxidation of Hastelloy S and Hastelloy C-4 in air at 600-800°C are now underway. The tests will last up to 10,000 hr. Initial results from the tests, up to 994 hr exposure, indicate that oxidation of the two alloys follows a parabolic rate relationship as expected based on earlier short-term test results. In Figures 13-14 Δm^2 (where Δm is the weight change/unit surface area) is plotted versus exposure time, and the straight line relationship indicates adherence to the parbolic rate law. Oxidation of the Hastelloy C-4 is more rapid than that of Hastelloy S throughout the temperature range studied. Both alloys form very adherent oxide layers at 600-800°C. A number of the test specimens were subjected to metallographic examination, and micrographs of the oxide-alloy interface of selected specimens are shown in

Figures 15 to 17. At 600 to 800°C the Hastelloy S forms a relatively uniform adherent oxide layer; however, there is some indication that preferential grain boundary attack may have occurred at 600 to 700°C. Some pitting was evident in the specimens exposed to air at 800°C. Additional examination of the specimens is planned to determine if grain boundary attack had occurred.

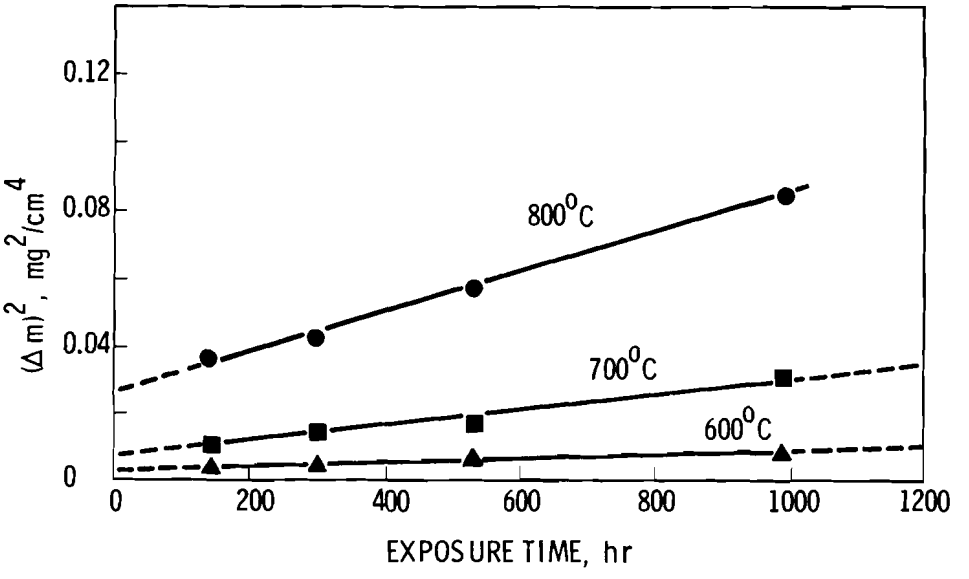

FIGURE 13. Oxidation of Hastelloy S at Various Temperatures

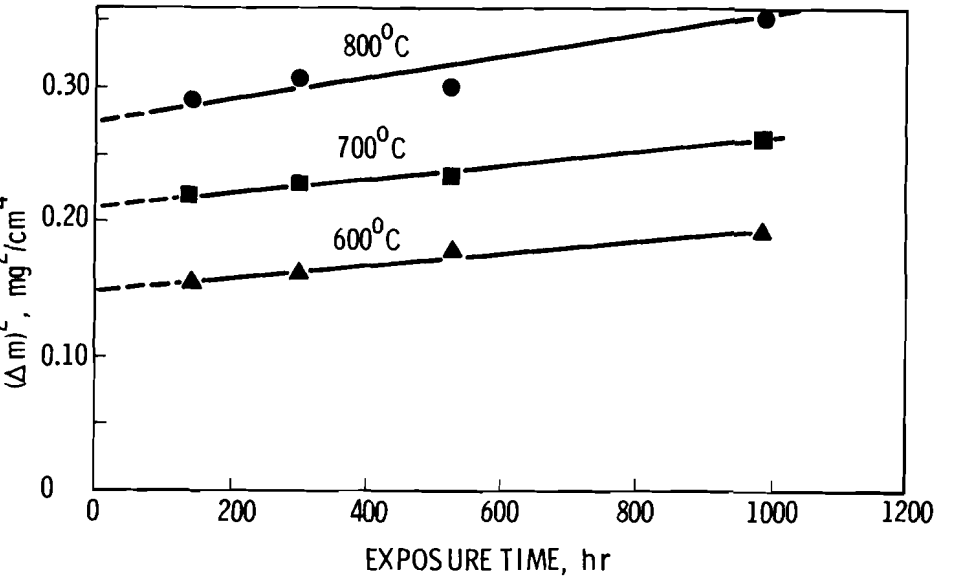

FIGURE 14. Oxidation of Hastelloy C-4 at Various Temperatures

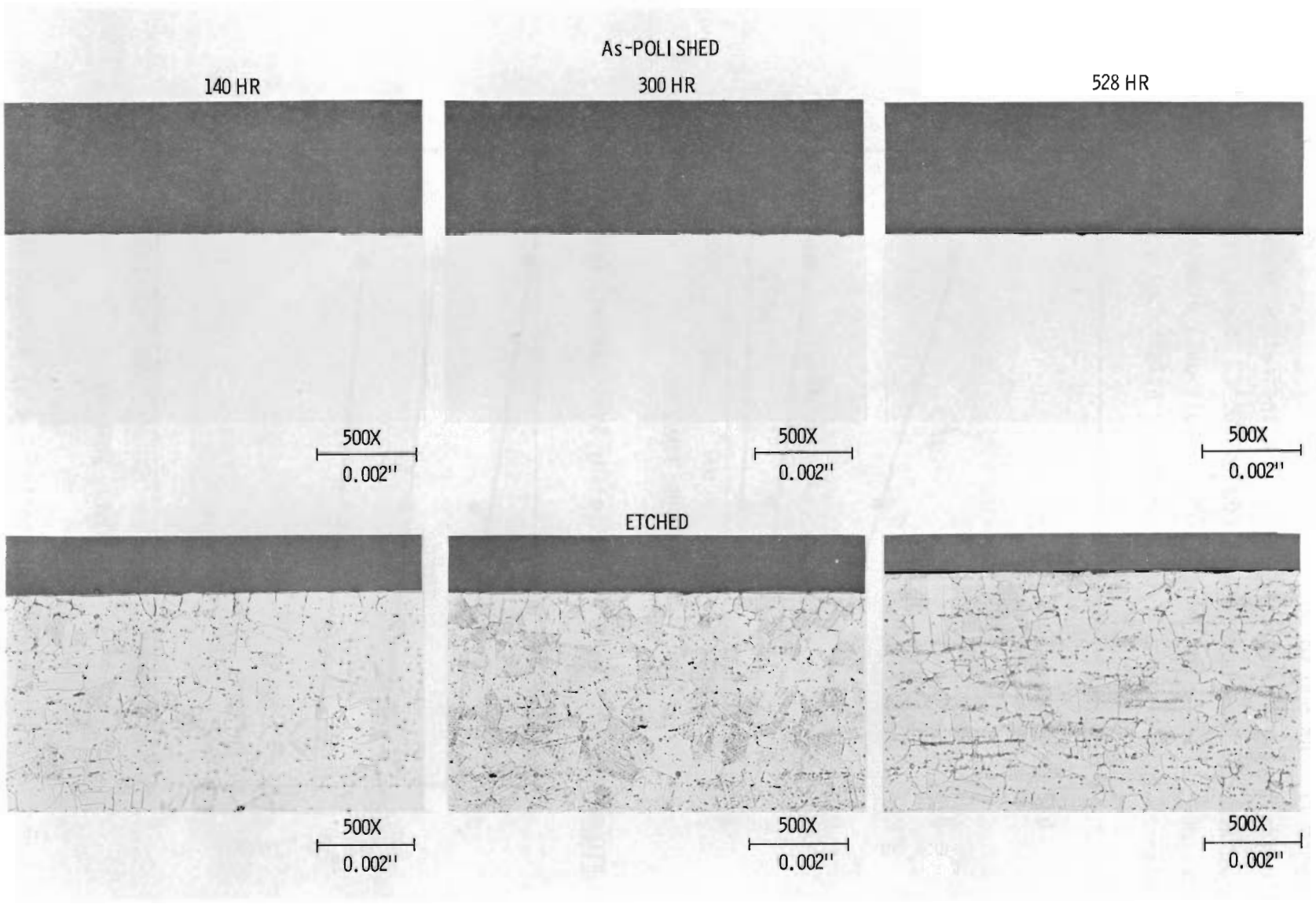

FIGURE 15. Hastelloy S Specimens Exposed to Air at 600°C

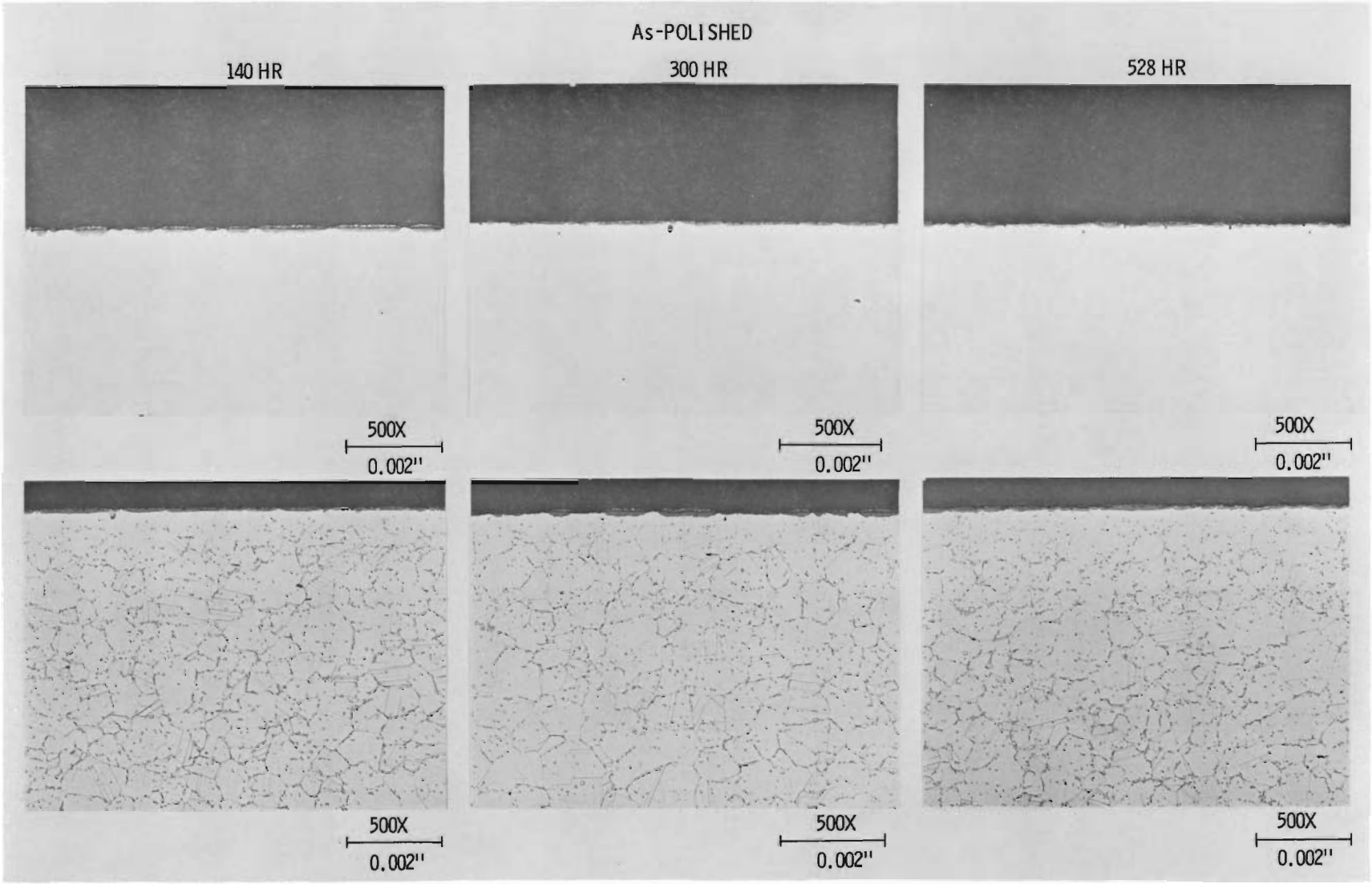

FIGURE 16. Hastelloy S Specimens Exposed to Air at 800°C

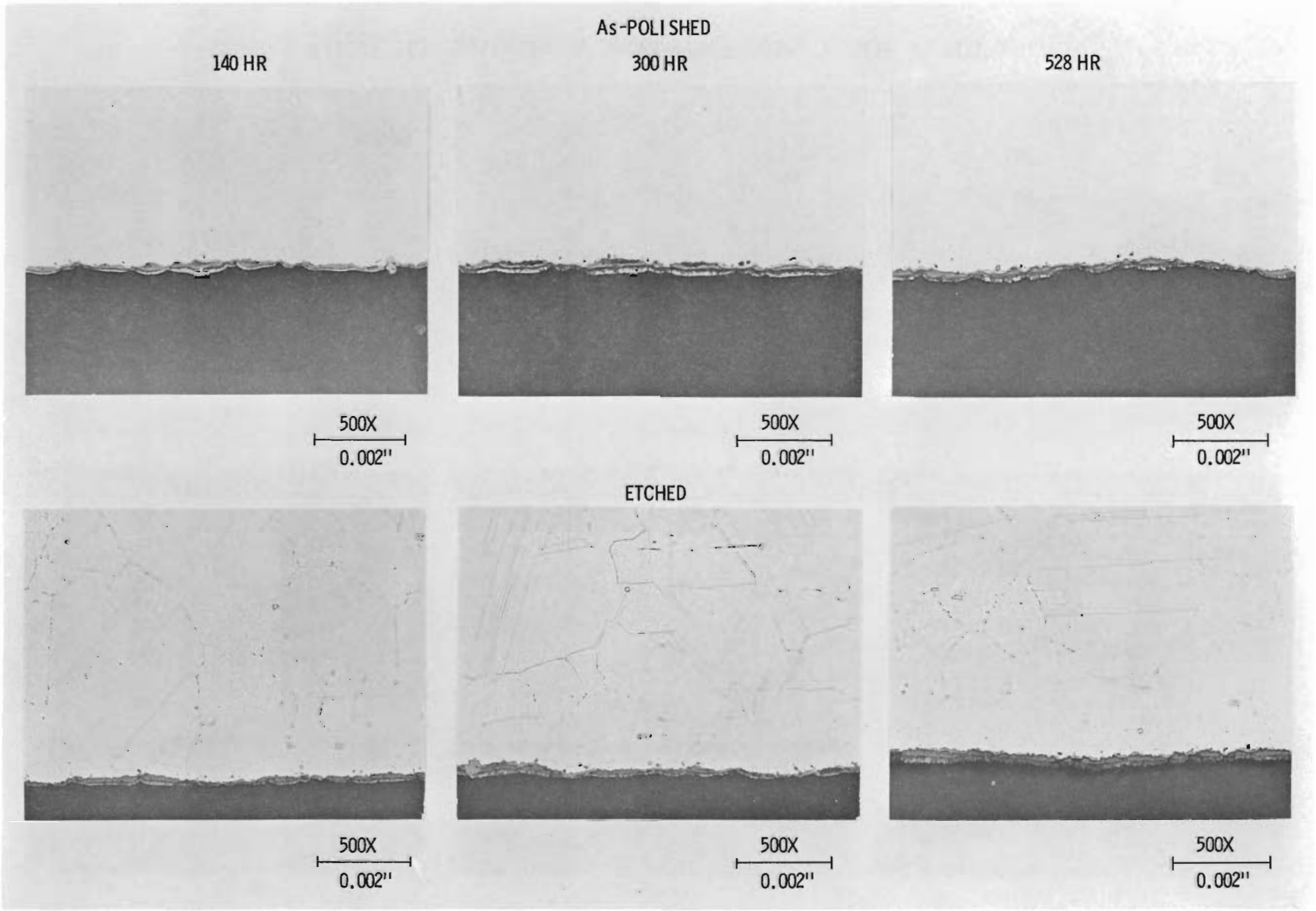

FIGURE 17. Hastelloy C-4 Specimens Exposed to Air at 800°C

Seawater Corrosion of Hastelloy S and Hastelloy C-4

Long-term tests are underway to measure the corrosion of Hastelloy S and Hastelloy C-4 in seawater. The tests are being carried out at the Battelle Facility at Sequim, WA and will last up to 10,000 hr. The test specimens are exposed to flowing seawater, taken from the Strait of Juan de Fuca, on a once-through basis in a covered polyethylene tank. Tensile specimens and pre-stressed specimens are being evaluated as well as standard corrosion strips. The tensile specimens used are similar to the 0.113" dia. ASTM subsize specimens used in the $^{90}SrF_2$ compatibility studies. The stressed specimens were cut from alloy plate in both the longitudinal and transverse directions. The corrosion strips were cut from the same plates as the stressed specimens. The nominal test periods are 250, 500, 1,000, 2,500, 5,000, 7,500, and 10,000 hr. Four Hastelloy S and three Hastelloy C-4 corrosion strips are being tested for each time period, while four tensile specimens of each alloy are under test for each of the last five time periods.

The initial results from the tests (250 hr exposures) indicate very little attack of the two alloys. The Hastelloy S specimens suffered an average weight loss of 0.004 mg/cm^2 while the Hastelloy C-4 specimens lost 0.068 mg/cm^2. Microscopic examination of Hastelloy S specimen surfaces showed no indication of pitting, grain boundary attack, or scale formation. The Hastelloy C-4 specimens exhibited a rust-colored scale which was easily removed with a bristle brush and soapy water. Microscopic examination of the specimens showed no evidence of pitting or grain boundary attack. Attack of the Hastelloy C-4 was greater than one would predict from earlier short-term tests, and this is the first time a scale layer has been observed with Hastelloy C-4 specimens exposed to seawater.

DISTRIBUTION

No. of Copies

DOE Chicago
Patent Attorney
9800 S. Core Ave.
Argonne, IL 60439
AA Churm

DOE Advanced Systems & Materials Production Division
Washington, DC 20545
TA Dillon
TJ Dobry, Jr.
TJ Holleman
AP Litman
JJ Lombardo
WC Remini
BJ Rock
NR Thielke

DOE
E201
Washington, DC 20545
JN Maddox

DOE Waste Management Division
Washington, DC
CA Cooley

DOE Oak Ridge Operations Office
P.O. Box E
Oak Ridge, TN 37830
DC Davis, Jr.

DOE Savannah River Operations Office
P.O. Box A
Aiken, SC 29801
WT Goldston

27 DOE Technical Information Center

No. of Copies

Battelle Columbus Laboratories
505 King Avenue
Columbus, OH 43201
CA Alexander
WR Pardue
WJ Zielenback

E.I. duPont deNemours and Co.
Savannah River Plant
Aiken, SC 29801
RH Bass

E.I. duPont deNemours and Co.
Savannah River Laboratory
Aiken, SC 29801
RT Huntoon

Electronics and Applied Physics Division
Building 347.3, AERE Harwell
Oxfordshire OX11 ORA
GREAT BRITAIN
EH Cooke-Yarborough

General Atomic Co.
P.O. Box 81601
San Diego, CA 92138
HC Carney

General Electric Company MSVD
P.O. Box 8555
Philadelphia, PA 19101
PE Brown

General Electric Company
Vallecitos Laboratory
P.O. Box 846
Pleasanton, CA 94566
GE Robinson

Los Alamos Scientific Laboratory
P.O. Box 1663
Los Alamos, NM 87544
SE Bronisz
RA Kent
RNR Mulford

No. of Copies

Monsanto Research Corporation
Mound Laboratory (DOE)
Nuclear Operations
P.O. Box 32
Miamisburg, OH 45342
WT Cave
R Dewitt

Department of the Army
Headquarters, U.S. Army
Facilities Engineering Support Agency
Fort Belvoir, VA 22060
H. H. Musselman, Tech Dir.

Naval Nuclear Power Unit
Code 70
Port Hueneme, CA 93043
Officer in Charge
Lt. JH Vogt

2 Naval Facilities Engineering Command
Office of Special Assistant-Nuclear Programs (04N)
200 Stovall Street
Alexandria, VA 22332
AA Arcuni

Oak Ridge National Laboratory
Oak Ridge, TN 37830
FN Case
RS Crouse
KW Haff
J Hammond
E Lamb
CL Ottinger
JC Posey
AC Schaffhauser

No. of Copies

Teledyne Energy Systems
110 W. Timonium Road
Timonium, MD 21093
P Dick
R Hannah
WA McDonald
P Vogelberger

Westinghouse Astronuclear Laboratory
P.O. Box 10864
Pittsburgh, PA 15236
C.C. Silverstein

ONSITE

3 DOE Richland Operations
WA Burns
WC Johnson
HE Ransom

8 Rockwell Hanford Operations
LI Brecke
HH Hopkins
LM Knights
EJ Kosiancic
CW Malody
JD Moore
HP Shaw
RW Spencer

Battelle-Northwest
DG Atteridge
DB Cash
MO Cloninger
GW Dawson
TF Demmitt
3 HT Fullam
JH Jarrett
RP Marshall
RE Nightingale
DE Olesen
NJ Olson
AM Platt
WE Sande

No. of
Copies

Battelle-Northwest (cont'd)
FA Simonen
HH Van Tuyl
5 Technical Information Files
Technical Publications